

ORIGINAL ARTICLE

Longitudinal profiling identifies co-occurring *BRCA1/2* reversions, *TP53BP1*, *RIF1* and *PAXIP1* mutations in PARP inhibitor-resistant advanced breast cancer

E. Harvey-Jones^{1,2,3†}, M. Raghunandan^{1†}, L. Robbez-Masson^{1†}, L. Magraner-Pardo¹, T. Alaguthurai², A. Yablonovitch⁴, J. Yen⁴, H. Xiao¹, R. Brough¹, J. Frankum¹, F. Song¹, J. Yeung¹, T. Savy¹, A. Gulati¹, J. Alexander¹, H. Kemp¹, C. Starling¹, A. Konde¹, R. Marlow¹, M. Cheang⁵, P. Proszek⁶, M. Hubank⁶, M. Cai⁴, J. Trendell², R. Lu², R. Liccardo², N. Ravindran¹, A. Llop-Guevara⁷, O. Rodriguez⁷, J. Balmana⁷, N. Lukashchuk⁸, M. Dorschner⁴, L. Drusbosky⁴, I. Roxanis¹, V. Serra⁷, S. Haider¹, S. J. Pettitt^{1*}, C. J. Lord^{1*} & A. N. J. Tutt^{1,2,3*}

¹The Breast Cancer Now Toby Robins Research Centre, The Institute of Cancer Research, London, UK; ²The Breast Cancer Now Research Unit, Guy's Hospital Cancer Centre, King's College London, UK; ³The City of London Cancer Research UK Centre at King's College London, UK; ⁴Guardant Health Inc., Redwood City, USA; ⁵Clinical Trials and Statistics Unit, The Institute of Cancer Research, London, UK; ⁶Clinical Genomics, The Royal Marsden Hospital, London, UK; ⁷Vall d'Hebron Institute of Oncology, Barcelona, Spain; ⁸AstraZeneca, Cambridge, UK

Available online XXX

Background: Resistance to therapies that target homologous recombination deficiency (HRD) in breast cancer limits their overall effectiveness. Multiple, preclinically validated, mechanisms of resistance have been proposed, but their existence and relative frequency in clinical disease are unclear, as is how to target resistance.

Patients and methods: Longitudinal mutation and methylation profiling of circulating tumour (ct)DNA was carried out in 47 patients with metastatic *BRCA1*-, *BRCA2*- or *PALB2*-mutant breast cancer treated with HRD-targeted therapy who developed progressive disease—18 patients had primary resistance and 29 exhibited response followed by resistance. Circulating tumour DNA (ctDNA) isolated at multiple time points in the patient treatment course (before, on-treatment and at progression) was sequenced using a novel >750-gene intron/exon targeted sequencing panel. Where available, matched tumour biopsies were whole exome and RNA sequenced and also used to assess nuclear RAD51.

Results: *BRCA1/2* reversion mutations were present in 60% of patients and were the most prevalent form of resistance. In 10 cases, reversions were detected in ctDNA before clinical progression. Two new reversion-based mechanisms were identified: (i) intragenic *BRCA1/2* deletions with intronic breakpoints; and (ii) intragenic *BRCA1/2* secondary mutations that formed novel splice acceptor sites, the latter being confirmed by *in vitro* minigene reporter assays. When seen before commencing subsequent treatment, reversions were associated with significantly shorter time to progression. Tumours with reversions retained HRD mutational signatures but had functional HRD based on RAD51 status. Although less frequent than reversions, nonreversion mechanisms [loss-of-function (LoF) mutations in *TP53BP1*, *RIF1* or *PAXIP1*] were evident in patients with acquired resistance and occasionally coexisted with reversions, challenging the notion that singular resistance mechanisms emerge in each patient.

Conclusions: These observations map the prevalence of candidate drivers of resistance across time in a clinical setting, information with implications for clinical management and trial design in HRD breast cancers.

Key words: breast cancer, PARP inhibitors, platinum, liquid biopsy, drug resistance, homologous recombination deficiency

*Correspondence to: Dr Stephen Pettitt, The Breast Cancer Now Toby Robins Research Centre, The Institute of Cancer Research, 237 Fulham Road, London SW3 6JB, UK

E-mail: Stephen.Pettitt@icr.ac.uk (S. J. Pettitt).

*Prof Christopher Lord, The Breast Cancer Now Toby Robins Research Centre, The Institute of Cancer Research, 237 Fulham Road, London SW3 6JB, UK

E-mail: Chris.Lord@icr.ac.uk (C. J. Lord).

*Prof Andrew Tutt, The Breast Cancer Now Toby Robins Research Centre, The Institute of Cancer Research, 237 Fulham Road, London SW3 6JB, UK

E-mail: Andrew.Tutt@icr.ac.uk (A. N. J. Tutt).

[†]EHJ, MR and LRM contributed equally and are listed alphabetically.

0923-7534/© 2024 The Author(s). Published by Elsevier Ltd on behalf of European Society for Medical Oncology. This is an open access article under the CC BY license (<http://creativecommons.org/licenses/by/4.0/>).

INTRODUCTION

Poly (ADP-ribose) polymerase (PARP) inhibitors (PARPi)^{1,2} and platinum chemotherapeutics now form part of the standard of care in homologous recombination-deficient (HRD) breast cancer.³⁻⁸ Although PARPis are able to elicit significant and sustained clinical responses in advanced disease,^{3,4} and adjuvant use can prevent recurrence and death,^{7,8} PARPi resistance is a growing clinical problem, especially in patients with advanced disease.⁹ Preclinical studies originally identified secondary intragenic mutations in *BRCA2* (i.e. 'reversion' mutations within the gene, in addition to the original pathogenic mutation, that restore the open reading frame and function of *BRCA2*) as a cause of PARPi and also platinum salt resistance.^{10,11} Subsequent clinical studies have shown that somatic reversion mutations in *BRCA1*, *BRCA2*, *RAD51C*, *RAD51D* or *PALB2* occur in cases of platinum and/or PARPi-resistant ovarian cancer and are also seen in cases of breast, pancreatic or prostate cancer after PARPi treatment.¹¹⁻¹⁷ In comparison to ovarian cancer, where there is some indication of the frequency of *BRCA1/2* reversion mutations,¹³ most reversions identified in breast cancer to date have been described in case reports and small cohorts assayed at single time points¹²; consequently, the relative contribution of reversion-based drug resistance in breast cancer is not known.¹⁸ Furthermore, not all cases of resistance to HRD-targeted therapy can be explained by reversion mutation, implying the occurrence of other molecular routes to resistance. Preclinical studies have established a series of candidate mechanisms of PARPi resistance that do not involve reversion, including restoration of homologous recombination (HR) via loss of TP53BP1/RIF1/Shieldin components,¹⁹⁻²⁴ increased replication fork stability,²⁵ alterations in PARP1 or PARG²⁶⁻²⁸ or upregulation of drug efflux pumps that reduce the amount of PARPi in the cell.²⁹⁻³¹ However, evidence that mutations in such genes are prevalent in metastatic breast cancer is absent.¹⁸

The approval of PARPi and platinum chemotherapy for the treatment of *BRCA1/BRCA2*-mutated breast cancer allows us to study mechanisms of resistance in real-world practice. Here, we characterised both reversions and other candidate resistance mechanisms at multiple time points across patients' treatment journey, using targeted DNA sequencing in patients *BRCA1/BRCA2*-mutated breast cancer where HRD-targeted therapy resistance emerged.

METHODS

Study design

The BTBC (Breakthrough Breast Cancer) study is a longitudinal blood and tissue sampling protocol conducted alongside standard of care therapy in breast cancer patients. Informed consent was given by patients and the study conducted according to national ethics committee approved protocol (REC No: 13/LO/1248, Guy's & St Thomas' Hospital). For this study, a subset of patients with known *BRCA1*, *BRCA2* or *PALB2* mutations were identified based on

Table 1. Cohort characteristics.

Characteristics	Group 1 (n = 18)	Group 2 (n = 7)	Group 3 (n = 22)
Age (years), median (range)	39.1 (25-54)	42.7 (33-59)	39.9 (25-58)
Stage at diagnosis, n (%)			
1	3 (16.7)	1 (14.3)	—
2	2 (11.1)	1 (14.3)	10 (45.4)
3	8 (44.4)	2 (28.6)	9 (40.9)
4	5 (27.8)	3 (42.8)	3 (13.6)
Histological classification, n (%)			
ER+HER2—	6 (33.3)	2 (28.6)	13 (59)
ER+HER2+	1 (5.5)	—	—
TNBC	11(61.1)	5 (71.4)	9 (40.9)
<i>BRCA1/BRCA2/PALB2</i> germline mutation, n (%)			
<i>BRCA1</i>	11 (61.1)	3 (42.8)	8 (36.3)
<i>BRCA2</i>	6 (33.3)	3 (42.8)	14 (63.6)
<i>PALB2</i>	1 (5.5)	—	—
<i>BRCA1/BRCA2/PALB2</i> somatic mutation, n (%)			
<i>BRCA1</i>	—	1 (14.3)	—
Prior (neo)adjuvant chemotherapy, n (%)			
Yes	11 (61.1)	4 (57.1)	20 (90.9)
No	7 (38.9)	3 (42.8)	2 (9.1)
Prior platinum containing (neo)adjuvant chemotherapy, n (%)			
Yes	3 (27.3)	1 (25)	6 (30)
No	8 (72.7)	3 (75)	14 (70)
Prior palliative chemotherapy lines, n (%)			
0	6 (33.3)	2 (28.6)	7 (31.8)
1	10 (55.6)	5 (71.4)	11 (50)
2	—	—	3 (13.6)
3	1 (5.5)	—	1 (4.5)
4	1 (5.5)	—	—
Prior platinum containing palliative chemotherapy, n (% of patients receiving palliative chemotherapy)			
Yes	5 (41.7)	2 (40)	11 (73.3)
No	7 (58.3)	3 (60)	4 (26.7)
WES from first available tumour samples evaluable for <i>BRCA1/BRCA2/PALB2</i> LOH, n (%)			
Yes	10 (55)	5 (71.4)	6 (27.2)
No	8 (44.4)	2 (28.5)	16 (68.1)
Evidence of <i>BRCA1/BRCA2/PALB2</i> LOH in WES from first available tumour samples, n (% of evaluable)			
Yes	8 (80)	5 (100)	3 (50)
No	2 (20)	—	3 (50)
WES from first available tumour samples evaluable for HRD scar score or mutational signature analyses, n (%)			
Yes	12 (66.6)	5 (71.4)	10 (45.4)
No	6 (33.3)	2 (28.5)	12 (54.5)
HRD scar score>42 or SBS3-positive samples, n (% of evaluable)			
Yes	11 (91.6)	5 (100)	10 (100)
No	1 (8.3)	—	—

ER, estrogen receptor; HER2, human epidermal growth factor receptor 2; HRD, homologous recombination deficiency; LOH, loss of heterozygosity; SBS3, somatic single base substitution signature 3; TNBC, triple-negative breast cancer; WES, whole exome sequencing.

genetic testing or other molecular profiling data collected as part of the study. Clinical histories were codified, and archival tissue samples retrieved where possible. Patient response to therapy was monitored clinically and radiologically, and at least one plasma sample was collected per patient in Group 1, with at least 2 pre and post resistance plasma samples and up to 7 longitudinal plasma samples collected in Groups 2 and 3.

ctDNA sequencing and analysis

Genomic variant calls from ctDNA, including SNV/Indel, gene level copy number data and rearrangements were

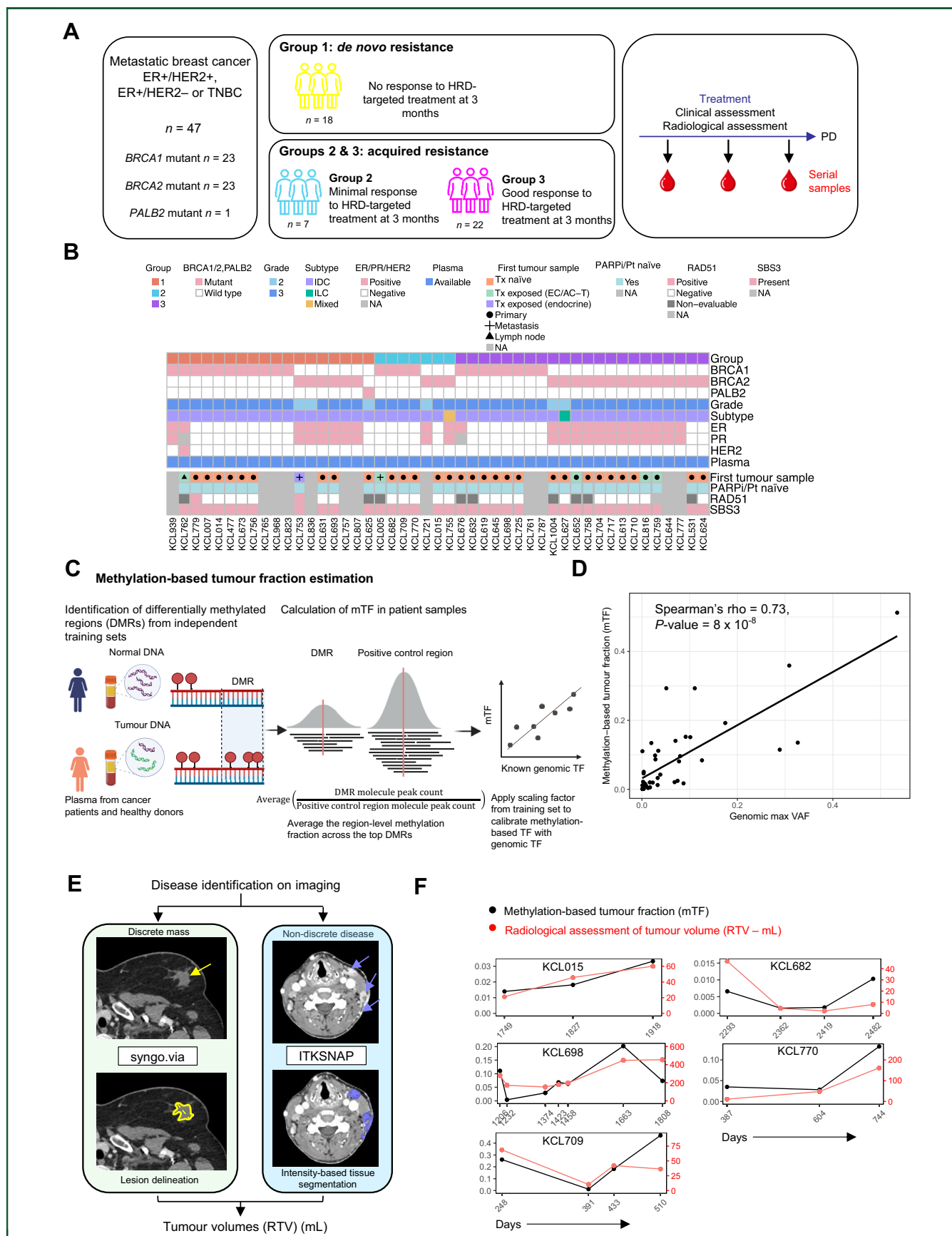


Figure 1. Study pipeline: HRD-targeted therapy in a cohort of patients with HR-deficient breast cancer. (A) Patient study schematic. Patients with metastatic breast cancer (ER+ PR+/- HER2- or TNBC) harbouring *BRCA1/2* or *PALB2* mutations were recruited to the study. Groups are defined as follows: Group 1—*de novo* resistance to HRD-targeted treatment at 3 months; Group 2—minimal response to HRD-targeted treatment at 3 months and Group 3—good response to HRD-targeted treatment at 3 months. (B) Patient baseline characteristics. Data were extracted from patient histopathology

generated using a commercial pipeline (Guardant Health) as previously described². To enrich for tumour specific mutations, somatic SNV/Indel calls were excluded if they were frequently identified in a database of commonly observed mutations associated with clonal haematopoiesis of indeterminate potential (CHIP). Variants were annotated as germline based on either the cfDNA result or other germline genetic testing information, if available.

Online content

Any additional methods are available at <https://doi.org/10.1016/j.annonc.2024.01.003>.

RESULTS

Patient characteristics

We collected tumour tissue and longitudinal blood plasma samples from 47 patients with either germline or somatic *BRCA1* ($n = 23$), *BRCA2* ($n = 23$) or *PALB2* ($n = 1$) mutant advanced breast cancer, who received treatment with PARPi and/or platinum agents (Table 1). All but one patient had a germline pathogenic mutation ($n = 46$). This patient had a somatic *BRCA1* mutation (Supplementary Table S1). We classified the platinum chemotherapy and/or PARPi responses in each patient into one of three clinically relevant groups: (i) Group 1—those with *de novo* resistance, that is, primary progression after no objective clinical and/or radiological response to HRD-targeted therapy at or before 3 months of treatment; (ii) Group 2—those with minimal response to treatment, that is, mixed response or stable disease at initial assessment followed by progressive disease; and (iii) Group 3—those with a good response to treatment, that is, complete response or partial response followed by progressive disease (Figure 1A). Patients may have received prior platinum chemotherapy, either in the (neo)adjuvant setting ($n = 10$) or in the advanced setting ($n = 18$; Supplementary Table S2, available at <https://doi.org/10.1016/j.annonc.2024.01.003>). Baseline patient characteristics, including HRD status as measured by the presence or absence of nuclear RAD51 foci³² and somatic single base substitution signature 3 (SBS3),³³ are shown in Figure 1B. Further details on treatment history can be found in Supplementary Figure S1A and B, available at <https://doi.org/10.1016/j.annonc.2024.01.003>. Where possible, blood samples for circulating tumour DNA (ctDNA) analysis were collected both before, during, and after developing resistance to HRD-targeted treatment (Figure 1A, Supplementary Figure S2A, available at <https://doi.org/10.1016/j.annonc.2024.01.003>, and Supplementary Table S3, available at <https://doi.org/10.1016/j.annonc.2024.01.003>).

In addition to isolating blood samples, we also obtained 80 tumour samples, collected either before or after resistance to HRD-targeting treatment; these were profiled using whole exome sequencing (WES) and whole transcriptome sequencing (RNA-seq) (Supplementary Figure S2B, available at <https://doi.org/10.1016/j.annonc.2024.01.003>).

In totality, we isolated 123 serial plasma samples from the 47 patients in the cohort and sequenced cell-free DNA (cfDNA) from these using a novel sequencing assay, GuardantINFINITY (Guardant Health). This assay reports single nucleotide variants (SNVs)/insertions/deletions (indels) from a panel of 753 genes and fusions in a subset of these genes. Most (40/47, 85%) patients had evidence of a pathogenic *TP53* mutation in ctDNA sequencing; frequencies of other metastatic breast cancer driver gene mutations³⁴ are shown in Supplementary Figure S3, available at <https://doi.org/10.1016/j.annonc.2024.01.003>. The gene set encompassed intron and exon coverage of 92 previously classified DNA damage response genes, including intronic coverage (Supplementary Figure S4, available at <https://doi.org/10.1016/j.annonc.2024.01.003>, Supplementary Tables S4 and S5, available at <https://doi.org/10.1016/j.annonc.2024.01.003>).³⁵⁻³⁷ We also compiled a consensus list of preclinically identified PARPi resistance genes from the published literature, including those identified via Clustered regularly interspaced palindromic repeats-CRISPR-associated protein 9 (CRISPR-Cas9) genetic perturbation screens in either *BRCA1*- or *BRCA2*-mutant cells, including three new PARPi resistance screens that we carried out (see the 'Methods' section and Supplementary Figure S5, available at <https://doi.org/10.1016/j.annonc.2024.01.003>, Supplementary Tables S6-S16, available at <https://doi.org/10.1016/j.annonc.2024.01.003>). The Guardant INFINITY gene panel contains 177 of these genes, including *SHLD1*, *TP53BP1*, *SHLD2*, *PARP1*, *STN1*, *TEN1*, *CTC1*, *RIF1*, *LIG4*, *XRCC4*, *ATMIN (ASCIZ)*, *DYNLL1*, *MAD2L2 (REV7)*, *ABC1*, *PAXIP1 (PTIP)*, *SLFN11*, *PARG* and *WRN*^{19,20,24,25,28,30,31,38-43} (Supplementary Figure S5J, available at <https://doi.org/10.1016/j.annonc.2024.01.003>). We successfully analysed 98.3% of the plasma samples collected ($n = 120$), generating a dataset of 29 samples (from 29 patients) collected before HRD-targeted therapy, 22 samples (from 13 patients) isolated during HRD-targeted treatment and 69 samples (from 47 patients) obtained after eventual progression (Supplementary Figure S2A, available at <https://doi.org/10.1016/j.annonc.2024.01.003>).

reports and electronic records. Data for the first available tumour sample are provided, acquired before PARPi or platinum exposure. Symbols indicate whether this was from primary breast tumour, regional lymph node or distant metastatic site. RAD51 status and HRD signature 3 (SBS3) status are reported. (C) Strategy for the estimation of mTF as a predictor of total ctDNA from plasma. (D) Scatter plot illustrating correlation between maximum somatic VAF of common breast cancer driver mutations in ctDNA versus mTF of study plasma samples successfully sequenced on GuardantINFINITY. R calculated by Spearman's correlation and significance using a t -test with 39 degrees of freedom. (E) Strategy for tumour volume estimation using 3D segmentation analyses from patient cross-sectional imaging during various stages of radiological assessment, matched to plasma time points. Disease is identified on cross-sectional imaging; lesions were measured using the indicated software and total tumour volume was estimated in millilitres. Yellow outlines and purple patches show how the lesion is segmented by the software. The purple arrows show contrast-enhancing areas that mark sites of disease involvement. (F) Line plots illustrating mirroring of mTF (black) derived from ctDNA analyses and tumour volume assessed using radiological assessment (RTV, red) over time in five patients.

ctDNA, circulating tumour DNA; ER, estrogen receptor; HER2, human epidermal growth factor receptor 2; HRD, homologous recombination deficiency; IDC, invasive ductal carcinoma; ILC, invasive lobular carcinoma; mTF, methylation-based tumour fraction; NA, not available; PARPi, poly (ADP-ribose) polymerase (PARP) inhibitor; PD, progressive disease; PR, progesterone receptor; RTV, radiologically assessed tumour volumes; TNBC, triple-negative breast cancer; VAF, variant allele frequency.

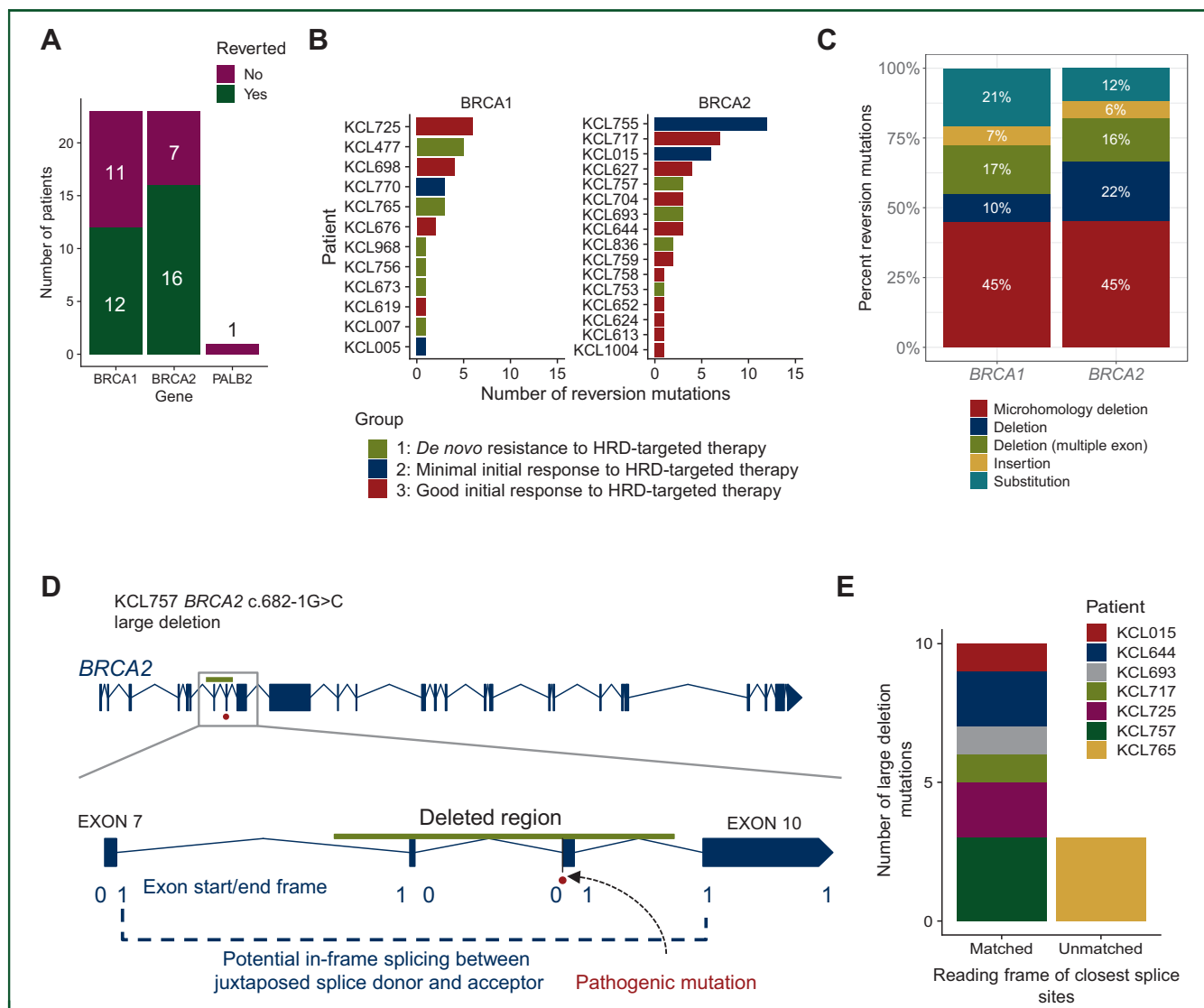


Figure 2. BRCA1/2 reversion mutations detected in the study.

(A) Bar chart summarising the number of patients with reversion mutations in BRCA1, BRCA2 and PALB2. (B) Bar chart summarising the number of reversion mutations identified per patient. (C) Bar chart of reversion mutation classifications. (D) Example of a large deletion in BRCA2 in KCL757. Intron/exon structure of BRCA2 is shown (top) with highlight on the exon 7 to exon 10 region (bottom). Deletion (green line) has break points in intronic sequences, encompasses the BRCA2 pathogenic mutation in exon 9 and is predicted to lead to an in-frame skipping of the pathogenic and neighbouring exons, juxtaposing a splice donor site flanking exon 7 and a splice acceptor site flanking exon 10. Numbers below each exon indicate their start and end phase. (E) Bar chart summarising the number of large BRCA1/2 deletions where deletions did (matched) or did not (unmatched) juxtapose exons that would splice in-frame. From 13 deletions identified, only three, all in KCL765, did not juxtapose in frame exons (Supplementary Figure S8, available at <https://doi.org/10.1016/j.annonc.2024.01.003>). HRD, homologous recombination deficiency.

and Supplementary Table S3, available at <https://doi.org/10.1016/j.annonc.2024.01.003>).

The majority of cfDNA in plasma is contributed by nonmalignant cells. The burden of ctDNA content within each patient's cfDNA sample was estimated using a methylation-based tumour fraction (mTF); mTF was calculated based on methylation levels across a set of genomic regions known to be methylated in tumour cells (Figure 1C; see the 'Methods' section). mTF correlated with the cfDNA variant allele frequency (VAF) of known somatic breast cancer driver mutations from the plasma samples in the cohort (Spearman's $\rho = 0.726$, $P = 8 \times 10^{-8}$; Figure 1D) and mirrored radiologically assessed tumour volume (Figure 1E and F; see the 'Methods' section). We therefore

used mTF as a measure of ctDNA content in plasma samples.

Reversion mutations are detected in plasma from the majority of patients with HRD-targeted therapy resistance

Taking the cohort as whole, we identified BRCA1 or BRCA2 reversion mutations in ctDNA from 60% of patients (28/47; Figure 2A) at the point of clinical resistance, making this the most commonly detected form of resistance. Reversion mutations were detected in ctDNA at VAFs ranging from 0.05% to 40%. In cases where both ctDNA sequencing and tumour WES were available, a low ctDNA VAF of reversions translated into much higher VAFs in WES (Supplementary

Figure S6A and B, available at <https://doi.org/10.1016/j.annonc.2024.01.003>), potentially due to the dilutional effect of nontumour ctDNA in plasma samples and/or lower ctDNA shedding from certain lesions. Sixteen patients in the cohort had multiple different reversions detected in their cfDNA in at least one time point. For example, in three patients with *BRCA2* mutations, we identified more than five different reversion mutations; one of these patients had 13 different reversion mutations (Figure 2B).

Most reversion mutations in the patient cohort were secondary deletion events; the majority of these secondary deletions had evidence of microhomology use at the deletion site (Figure 2C). Microhomology-flanked deletions are one feature of the distinct mutational signature seen in HR-deficient cancers, along with certain single base substitution signatures such as SBS3.³³ Genomic patterns of copy number loss, another feature of HRD tumours, are now used in clinically approved assays to direct the use of PARPi treatment in ovarian cancer.^{44,45} We examined single base substitution signatures in WES data from solid tumour biopsies with identified *BRCA1/2* reversion mutations (six patients). As expected, we saw extensive contribution of SBS3, which persisted even in resistant tumour biopsies carrying reversion mutations (Supplementary Figure S6C, available at <https://doi.org/10.1016/j.annonc.2024.01.003>). This is consistent with the idea that HRD-associated mutational scars do not necessarily report the current functional HR status and therefore are poor predictors of therapy sensitivity of a tumour, as is also the case for *BRCA1* methylation and its reversal.⁴⁶⁻⁴⁹ Consistent with restoration of HR function despite the presence of SBS3, we also saw evidence of restoration of nuclear RAD51 foci in all but one patient in post-HRD-targeted treatment resistance samples, when compared with treatment-naïve samples ($P < 0.001$; Supplementary Figure S6D, available at <https://doi.org/10.1016/j.annonc.2024.01.003>); this included paired samples with/without reversions ($P = 3.55 \times 10^{-8}$; Supplementary Figure S6E, available at <https://doi.org/10.1016/j.annonc.2024.01.003>), also suggesting that RAD51 foci are more representative of the functional HR status of the tumour than the presence of an historical HRD genomic scar in the tumour genome.³²

Most previously described reversion mutations in *BRCA1* or *BRCA2* involve deletion of <100 bp of coding sequence within a single exon¹²; this apparent property of reversions may be due to HRD-targeted therapy selecting for reversion events that reconstitute close-to-wild-type *BRCA1* or *BRCA2* coding sequences. Alternatively, this could be due to the widespread use of exon capture panels that do not reliably detect larger deletions, such as those with breakpoints outside exons. As the GuardantINFINITY panel covers all *BRCA1* and *BRCA2* introns (except repetitive sequences; see Supplementary Table S4, available at <https://doi.org/10.1016/j.annonc.2024.01.003>), it is capable of detecting larger genomic deletions with intronic breakpoints in *BRCA1* or *BRCA2*. We noted that 13 reversion mutations from seven patients (17% and 16% of all reversions detected in *BRCA1* and *BRCA2*, respectively; Figure 2C) occurred via a

large deletion not contained within a single exon, with at least one breakpoint in an intron (Supplementary Figure S7, available at <https://doi.org/10.1016/j.annonc.2024.01.003>). These deletions always affected the exon containing the patient's pathogenic mutation or nearby sequences, suggesting that they are a mechanism for removal or modulation of the pathogenic mutation. For example, a deletion in patient KCL757 resulted in deletion of part of *BRCA2* intron 7, all of exon 8, intron 8, the entire exon with the pathogenic splice acceptor mutation (*BRCA2* exon 9) and part of intron 9 (Figure 2D). We therefore considered whether these deletions might lead to alternative splice events that bypassed the pathogenic mutation. For this to be the case, the start and end reading frames of the closest intact exons flanking the deletion should be matched, suggesting that if these were spliced together by a novel splicing event, an in-frame protein would be encoded. This was the case in all but one patient (Figure 2E and Supplementary Figure S7, available at <https://doi.org/10.1016/j.annonc.2024.01.003>).

Reversion mutations leading to new splicing events

We found further evidence for the role of *BRCA1/2* splicing changes in the context of resistance in our cohort. One patient, KCL015, with a *BRCA2*:c.7008-1G>A exon 14 splice acceptor pathogenic mutation, had three distinct second-site SNV mutations at the start of exon 14 (within the coding sequence) and two distinct second-site 8-bp deletions in the preceding exon 13, detected in the ctDNA sample at the point of therapeutic resistance (Figure 3A). The second-site SNV mutations (M1: c.7010C>G, M2: c.7013C>G, M3: c.7016A>G) present at resistance were each in *cis* with the pathogenic mutation but did not co-occur on the same sequencing read, suggesting that each secondary mutation was an independent event. As the second-site mutations were spaced in 3-bp intervals and 3' of an adenine, they could each conceivably restore an 'AG' consensus splice acceptor site in the correct reading frame to restore exon 13/exon 14 splicing. To test the ability of these second-site mutations to restore splicing to a *BRCA2*:c.7008-1G>A allele, we constructed a reporter plasmid containing the distal regions of intron 13 (including the c.7008-1G>A mutation) and fragments of the flanking exons 13 and 14 fused in-frame to a luciferase reporter gene (Figure 3B). The plasmid reporter with the pathogenic mutation alone showed greatly reduced luciferase expression compared with the wild-type sequence (Figure 3C). The luciferase signal was restored by each of the additional secondary *BRCA2* mutations, indicating that these could restore functional splicing (Figure 3C). Sequencing complementary DNA prepared from transfected cells confirmed use of the positions with the reversion mutations as novel splice acceptors leading to in-frame splicing (Figure 3D-F). The 8-bp exon 13 deletions (US1 and US2) led to the use of the canonical exon 13 splice donor with a noncanonical exon 14 splice acceptor site 10-bp downstream of the (pathogenic mutation) native splice acceptor, thus retaining

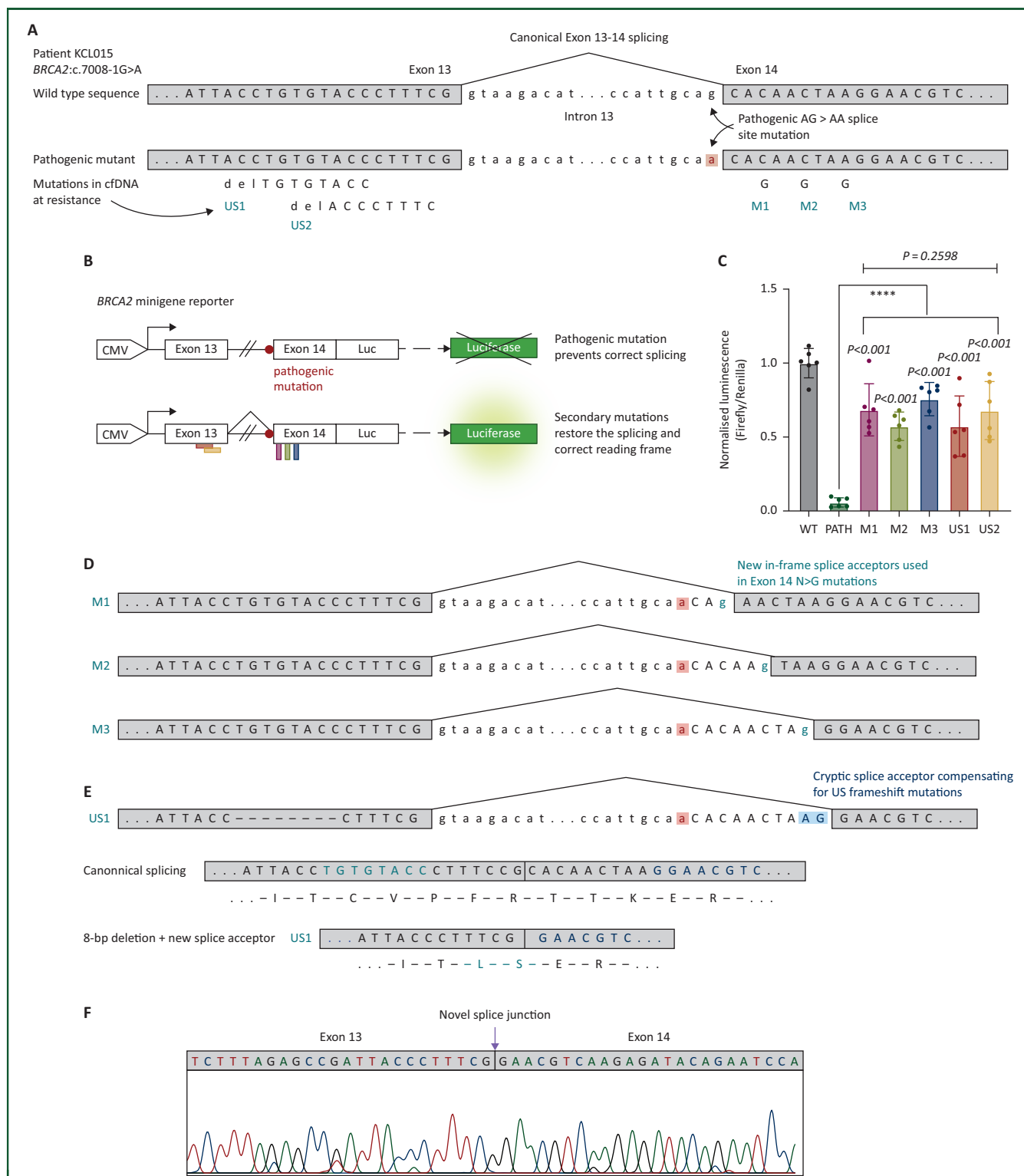


Figure 3. Reversion of splice site mutations. (A) Partial sequence of *BRCA2* (exon 13/partial intron/exon 14) in patient KCL015 showing positions of pathogenic AG>AA splice acceptor site mutation and secondary somatic mutations: downstream single base substitutions (M1, M2 and M3) and upstream 8-bp deletions (US1 and US2). (B) Schematic of the *BRCA2* minigene reporter used to confirm splicing events caused by M1, M2, M3, US1 and US2. Top: A CMV promoter was fused to a *BRCA2* exon 13–intron–exon 14 DNA sequence encompassing the pathogenic AG>AA splice acceptor site mutation and a 3' luciferase coding sequence (Luc). Presence of the AG>AA mutation (red dot) prevented splicing and encoding of luciferase. Bottom: additional constructs were constructed, including individual mutations US1, US2, M1, M2 and M3 along with the pathogenic mutation. (C) Bar chart showing luciferase signal from HEK293T cells transfected with constructs described in (B). US1, US2, M1, M2 and M3 are constructs with *BRCA2* AG>AA mutation sequence and secondary mutations. Error bars represent standard deviation; *P* values calculated via an unpaired *t* test. (D) Spliced sequence of *BRCA2* minigene (exon 13/partial intron/exon14) observed from mRNA RT-PCR/sequencing of HEK293T cells transfected with M1, M2 and M3 minigene reporters in the experiment shown in (C). PCR was carried out using a forward primer in exon 13 and a reverse primer in Luc. Mutations reconstitute exon 13/14 splicing using new in-frame AG splice acceptor sites in exon 14, as shown. (E) Splicing of *BRCA2* (exon 13/partial intron/exon14) observed from mRNA RT-PCR/sequencing of HEK293T cells transfected with the US1 minigene reporter. The 8-bp US1 deletion alters the native frame of *BRCA2* and allows the use of a preexisting cryptic AG splice

exon 14 (Figure 3E-F). Similar changes may explain the mechanism of resistance in patient KCL765, where large deletions of regions surrounding the pathogenic splice donor were observed, but the phases of adjacent exons were not consistent with straightforward use of canonical splice sites (Figure 2E and Supplementary Figure S8, available at <https://doi.org/10.1016/j.annonc.2024.01.003>). In two of the three mutations in this patient, a novel potential AG acceptor site was introduced in the *BRCA1* allele with the large deletion, raising the possibility that noncanonical splicing is also a mechanism to restore *BRCA1* function in this case (Supplementary Figure S8, available at <https://doi.org/10.1016/j.annonc.2024.01.003>).

TP53BP1, RIF1 and PAXIP1 mutations occur in patients at progression on PARPi

We next looked for evidence of mutations in our consensus list of candidate genes involved in PARPi resistance, identified in preclinical experiments (Supplementary Figure S5, available at <https://doi.org/10.1016/j.annonc.2024.01.003>). We identified LoF mutations (frameshift, nonsense or splice site mutations) in *TP53BP1*, *RIF1* and *PAXIP1* (*PTIP*) in samples taken at PARPi resistance (Figure 4A). Defects in *53BP1* and *RIF1* are associated with the restoration of DNA end resection and HR in *BRCA1m* cells,^{20,50-52} whereas LoF of *PAXIP1* has been shown to lead to replication fork stabilisation and cisplatin or PARPi resistance in *Brca2*-mutant mouse cells.²⁵ Four *BRCA1m* patients (KCL698, 725, 762 and 709) had detectable deleterious mutations in *TP53BP1*, *RIF1*, or both, in ctDNA at treatment resistance (Figure 4A and Supplementary Figure S9A and B, available at <https://doi.org/10.1016/j.annonc.2024.01.003>). Two *BRCA2m* patients (KCL015 and 777) had deleterious *PAXIP1* mutations in ctDNA after carboplatin or olaparib resistance, respectively (Figure 4A and Supplementary Figure S9C, available at <https://doi.org/10.1016/j.annonc.2024.01.003>). One *BRCA2m* patient had a *TP53BP1* nonsense mutation, although it is not known what role *53BP1* might play in resistance in a *BRCA2m* context. None of these mutations were detected in samples taken from the same patients before the development of resistance. These findings suggest that these preclinically identified mechanisms of resistance do operate clinically. Unexpectedly, these *TP53BP1*, *RIF1* and *PAXIP1* mutations were often detected in who also had concurrently with reversion mutations in *BRCA1/2* (Figure 4A). This is of potential relevance for therapy approaches that target such pathways but assume continued loss of *BRCA1* function such as Pol-theta inhibitors.⁵³

To determine the dynamics of emergence of each of these resistance mechanisms (Figure 4A), we assessed the frequency of resistance-causing mutations in samples taken longitudinally through the patient's treatment course. For

example, we analysed three plasma samples (P1–P3) from patient KCL015 (germline *BRCA2*: c.7008-1G>A; Figure 4B): P1 after carboplatin induction but before olaparib treatment, P2 upon olaparib resistance, and P3 after progression on subsequent carboplatin rechallenge (Figure 4B). Both the ctDNA mTF measure of tumour burden and radiologically assessed tumour volume increased at progression on olaparib and on subsequent carboplatin rechallenge (P2 and P3; Figure 4C). We also observed the emergence of six unique *BRCA2* reversion mutations predicted to restore splicing of *BRCA2* (Figures 3 and 4D and E) as well as a frameshift *PAXIP1* mutation (p.M549fs; Figure 4D and E and Supplementary Figure S9C, available at <https://doi.org/10.1016/j.annonc.2024.01.003>). *BRCA2* reversion and *PAXIP1* mutation could each contribute towards stabilisation of carboplatin-stalled replication forks and potentially increase the fitness of cells under selective pressure from DNA-damaging treatment.

We also identified the presence of multiple, apparently co-existing, mechanisms of therapeutic resistance in patient KCL698 (germline *BRCA1*:c.4327C>T, p.R1443*), where *BRCA1* reversions as well as *RIF1* and *TP53BP1* mutations were seen at different times during the patient's treatment history (Figure 4F). We analysed plasma samples at the start of olaparib treatment (P1), during a good response to olaparib (P2, P3 and P4), at clinical progression on olaparib (P5), before carboplatin rechallenge (P6) and then following demonstration of carboplatin resistance (P7; Figure 4F). In the plasma sample taken before clinical detection of PARPi resistance (P4), we detected a *BRCA1* reversion mutation (c.4327C>G) and a truncating mutation in *TP53BP1* (p.Q240*; Figure 4G and H). At clinical progression on olaparib (P5), we noted the emergence of a truncating *RIF1* mutation (p.A1176fs) and an additional *BRCA1* reversion mutation (c.4329A>G) that was also detected in a temporally matched WES from a breast tumour (Specimen B; Figure 4F-H). The reversion mutation observed in the post-olaparib resistance biopsy (Specimen B) leads to restoration of HR as indicated by the appearance nuclear RAD51 and *BRCA1* foci detected by a *BRCA1*-C-terminal antibody (Figure 4I and J). At PARPi resistance, before a rechallenge with carboplatin because of a prior demonstration of response (P6), we observed a total of four *BRCA1* reversions and the *TP53BP1* truncating mutation but could no longer detect the *RIF1* mutation (Figure 4F-H). In the last plasma sample after rechallenge with carboplatin (P7), three of the reversion mutations persisted but neither the *TP53BP1* nor *RIF1* mutations were detected. This observation raises an interesting hypothesis: that in the absence of a PARPi selective pressure and faced with a carboplatin challenge, *BRCA1* reversion mutations are selected over mutations that result in loss of the NHEJ pathway proteins such as those in *53BP1* and *RIF1*. It is possible that NHEJ pathway mutations

acceptor site in exon 14, changing the predicted amino acid sequence as shown. (F) Sanger **** P<0.0001 sequencing trace of the transcript generated from the *BRCA2*–US1–luciferase reporter plasmid showing the novel exon 13/14 splice junction.

CMV, cytomegalovirus; mRNA, messenger RNA; PATH, construct with *BRCA2* AG>AA mutation sequence; WT, construct with *BRCA2* wild-type sequence.

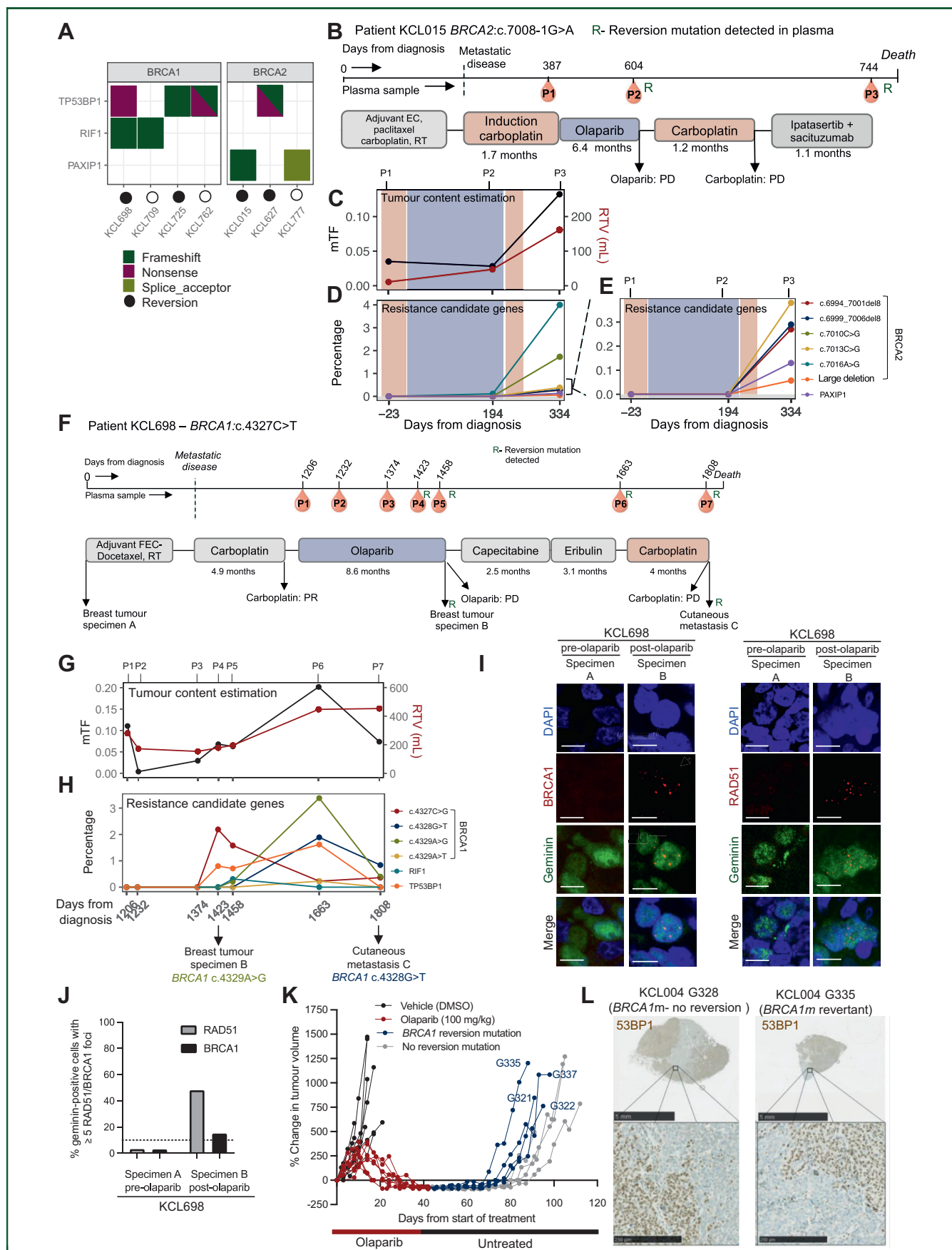


Figure 4. Co-occurrence of multiple mechanisms of HRD-targeted therapy resistance. (A) Heatmap illustrating presence of deleterious *TP53BP1*, *RIF1* and *PAXIP1* mutations detected in patients after resistance to PARPi/carboplatin ctDNA. Co-occurrence of *BRCA1/2* reversions is highlighted. (B) Schematic of clinical history of a *BRCA2*-mutant patient KCL015; red drops indicate times of blood draw for plasma sampling. Duration of each treatment delivered in metastatic setting is indicated in

confer a fitness advantage under PARPi selective pressure but are outcompeted by reversion mutations during other treatment. In the tumour biopsy samples from this patient we found two of the *BRCA1* reversions detected in ctDNA (c.4329A>G and c.4328G>T), one in each of two temporally and spatially separated biopsies (breast tumour specimen B versus cutaneous metastasis specimen C located in the right inframammary fold), indicating that the multiple mutations observed in ctDNA may represent mutations emerging from subclones at different sites (Figure 4F-H).

Validation of parallel evolution of resistance mechanisms using a *BRCA1*-mutant patient-derived xenograft model

The presence of multiple mechanisms of PARPi resistance in the same patient raised the possibility of emergence of parallel evolutionary paths to resistance. To test this prospectively, we modelled the emergence of resistance in a patient-derived xenograft model derived from a treatment-naïve tumour from patient KCL004 with a pathogenic *BRCA1* germline mutation. This patient received adjuvant chemotherapy but had not developed advanced disease in 6.9 years of follow-up and was therefore not included in the HRD-targeted therapy-resistant cohort described here. Mice with implants of KCL004's patient-derived xenograft were treated with either olaparib or drug vehicle for 42 days until the tumours had regressed in the olaparib-treated arm and then allowed to regrow without treatment (Figure 4K). Four of eight outgrowths analysed had *BRCA1* reversion mutations (Supplementary Figure S10A and B, available at <https://doi.org/10.1016/j.annonc.2024.01.003>) accompanied by restoration of *BRCA1* and *RAD51* foci (Supplementary Figure 10C-E, available at <https://doi.org/10.1016/j.annonc.2024.01.003>), whereas other outgrowths had distinct regions of 53BP1 loss (detected by IHC), in the absence of reversion. Notably, in two outgrowths, both reversions and loss of 53BP1 IHC were seen, confirming that reversion and nonreversion-based mechanisms of resistance can emerge, in parallel, from the same original tumour (Figure 4K and L and Supplementary Figure 10A, available at <https://doi.org/10.1016/j.annonc.2024.01.003>).

Resistance in the absence of reversion mutations

We reasoned that resistance mechanisms other than reversion mutations might be more likely in patients where

the pathogenic mutation would not be amenable to reversion-driven resistance. These could include *BRCA1/2* pathogenic mutations that are large genomic rearrangements, missense pathogenic mutations or mutations in the *BRCA2* C-terminus^{12,54,55} (Supplementary Table S17, available at <https://doi.org/10.1016/j.annonc.2024.01.003>, Figure 5A and B). One patient in our cohort (KCL709) had a somatic rearrangement in *BRCA1* (an inversion involving *EZH1*; Supplementary Figure S11A, available at <https://doi.org/10.1016/j.annonc.2024.01.003>). We analysed matched plasma and tumour samples before (P1 and breast tumour specimen T1), during (P2) and after olaparib resistance (P3 and P4, breast tumour specimen T2 and brain metastasis specimen S1–S3; Figure 5C-F). Scans at matched times showed progression in the breast tumour on olaparib, followed by the development of intracranial metastatic disease (Figure 5C and D). The GuardantINFINITY assay detected *BRCA1* promoter methylation across all evaluable plasma samples, suggesting a mechanism by which the nonrearranged *BRCA1* allele might be silenced in this patient's tumour, as occasionally observed previously.^{56,57} Bisulfite amplicon sequencing confirmed high levels of *BRCA1* promoter methylation in both pre- and post-olaparib resistance breast tumour specimens; the brain lesion was unevaluable in this assay (Supplementary Figure S11B, available at <https://doi.org/10.1016/j.annonc.2024.01.003>). Consistent with this, RNA-seq analysis revealed that pre-olaparib breast tumour specimen T1 and brain metastasis specimen S1–S3 had the lowest *BRCA1* messenger RNA (mRNA) expression across tissue samples from the entire cohort (Figure 5G), whereas olaparib-resistant breast tumour specimen T2 had higher *BRCA1* mRNA expression, despite the high level of *BRCA1* promoter methylation. Consistent with the restoration of *BRCA1* mRNA expression, we noted restoration of *BRCA1* and *RAD51* foci in olaparib-resistant breast specimen 2, when compared with the low *BRCA1*-mRNA expressing samples: pre-olaparib breast tumour specimen T1 and brain metastasis specimen S3 (Figure 5H-K, Supplementary Figure S10C-E, available at <https://doi.org/10.1016/j.annonc.2024.01.003> for imaging controls). The increased expression of *BRCA1* mRNA and protein, despite persistence of *BRCA1* methylation in breast tumour specimen T2, suggested the presence of at least one resistant subclone of the tumour with restored *BRCA1* expression through an unknown mechanism.

months. (C) Line plot showing change in methylated tumour fraction (mTF) and RTVs across the treatment duration. Orange shading, time during carboplatin treatment; lilac shading, time during olaparib treatment. P1-3 indicate the points at which plasma ctDNA was isolated. (D) Line plot showing the presence of *BRCA1* reversion and *PAXIP1* loss-of-function mutations in KCL015 ctDNA over the same period. (E) Zoomed-in view of the mutations detected at <0.5%. (F) Schematic of clinical history of *BRCA1*-mutant patient KCL698; details per (B). (G) Line plot showing change in mTF and RTV across the treatment duration; details per (C). (H) Line plot showing percentages of *BRCA1* reversion, *TP53BP1* and *RIF1* loss-of-function mutations in KCL698 over the duration of treatment. Two distinct *BRCA1* reversion mutations were detected from spatially and temporally distinct biopsies (breast biopsy B and cutaneous nodule C). (I) Confocal microscopy images of KCL698 FFPE tumour specimens isolated before and after olaparib resistance. *RAD51* and *BRCA1* foci in geminin-positive cells are shown. Scale bar = 10 µm. (J) Quantification of (I). A *RAD51* score of >10% indicates homologous recombination proficiency. (K) Emergence of tumour outgrowths after olaparib treatment in a PDX model of *BRCA1*-mutant breast cancer. Treatment-naïve PDX derived from a *BRCA1*-mutant patient was implanted in recipient mice; once tumours measured 50 mm³, they were treated with vehicle or 100 mg/kg of olaparib for 42 days. After cessation of treatment, mice were left untreated and monitored for tumour relapse. Each line represents an individual animal with tumour volume shown relative to treatment day 0. Tumour outgrowths harbouring *BRCA1* reversion mutations are indicated in blue (G335, G337, G321 and G322); outgrowths without reversions are labelled in grey. (L) Tumour micrographs illustrating spatial loss of 53BP1 immunohistochemical staining in PDX-G328 and G335 tumour outgrowths, respectively.

ctDNA, circulating tumour DNA; FFPE, formalin-fixed, paraffin-embedded; HRD, homologous recombination deficiency; mTF, methylation-based tumour fraction; PARPi, poly (ADP-ribose) polymerase (PARP) inhibitor; PDX, patient-derived xenograft; RT, radiotherapy; RTV, radiologically assessed tumour volumes.

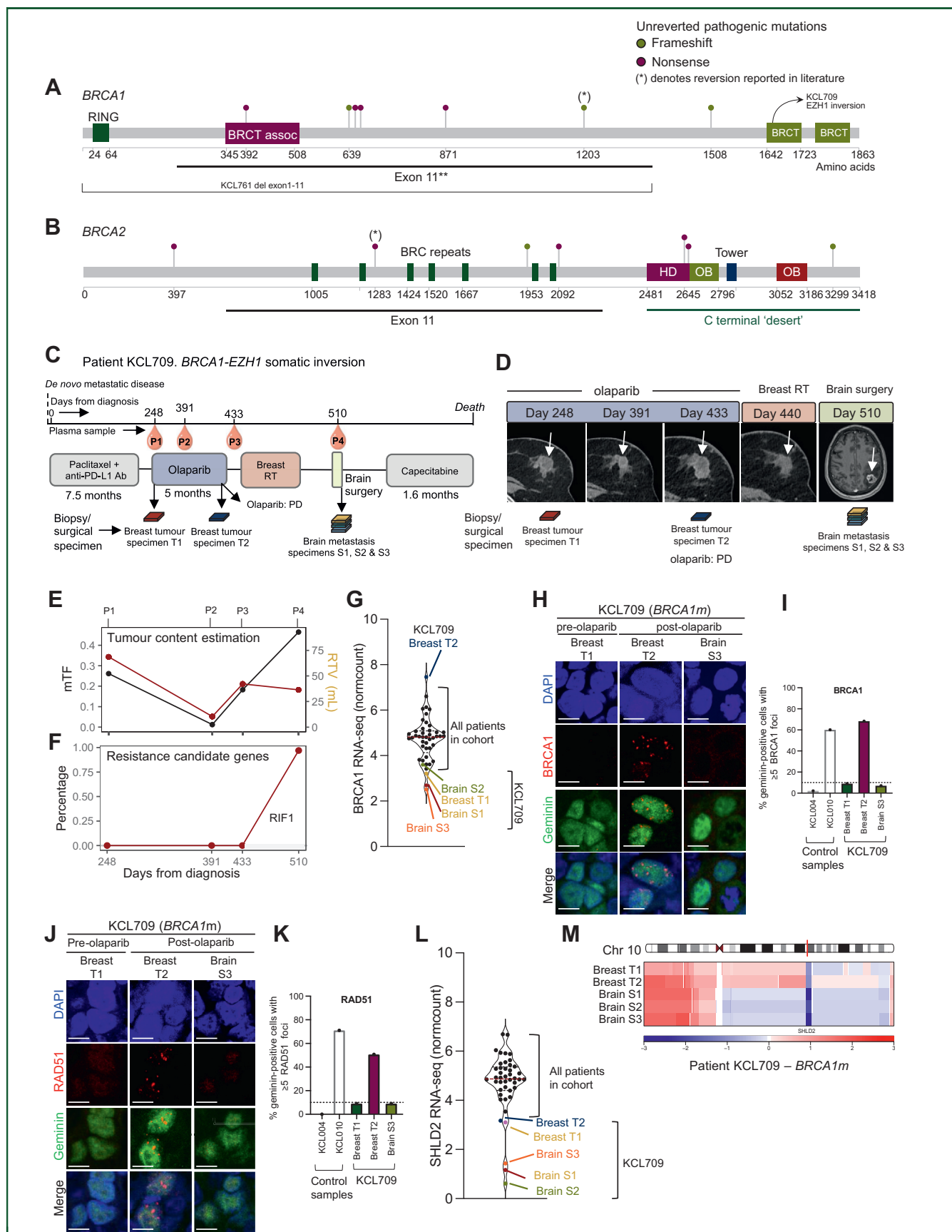


Figure 5. Development of clinical resistance to HRD-targeted therapy in the absence of reversion mutations. (A, B) Domain structures of (A) *BRCA1* and (B) *BRCA2* proteins annotated with the position of pathogenic mutations that did not revert in PARPi-resistant patient samples. (C) Schematic of clinical history of patient KCL709 who possessed a somatic *BRCA1-EZH1* rearrangement and *BRCA1* promoter methylation. Red drops indicate times of blood draw and arrows mark tumour biopsies or surgical tumour specimens: breast tumour specimen T1 (breast biopsy before olaparib), breast tumour specimen T2 (breast biopsy after olaparib PD) and brain

In plasma sample P4, matched to the detection of brain metastasis (where no BRCA1 restoration was seen), we observed emergence of an *RIF1* truncating mutation, p.T1013fs, in the ctDNA (Figure 5E and F); this was at low VAF and not observed in the contemporaneous tumour biopsy, suggesting that it may only be present in certain lesions or subclones. All breast and brain specimens also showed evidence of low *SHLD2* mRNA expression and *SHLD2* copy number loss (Figure 5L and M). Overall, these data suggest several potential mechanisms that may be contributing to resistance in this patient where a genetic reversion of *BRCA1* is not possible. The prevalence and validation of nonreversion-based resistance in the setting of pathogenic *BRCA1/2* alleles unamenable to reversion requires further study.

Presence of reversion mutations is associated with shorter time to progression on olaparib therapy

Finally, we assessed whether the mechanisms of resistance (both reversion and non-reversion forms) differed depending on whether the patients responded to their HRD-targeted therapy, that is, between Groups 1, 2 and 3. We found that 62.5% of patients with available baseline plasma samples in Group 1 (*de novo* resistant) had a detectable resistance mechanism at baseline, all of which were reversion mutations. By contrast, in those demonstrating mixed response, stable disease or objective response (partial or complete response; Groups 2 and 3), there was no evidence of reversions or any other mechanism of resistance in samples taken before HRD-targeted therapy (Figure 6A). After clinical resistance was observed, reversions were common in all groups, being seen in 56%, 57% and 64% of Group 1, Group 2 and Group 3, respectively (Figure 6B).

We next queried whether the detection of resistance mechanisms in ctDNA before treatment was associated with treatment response. Of the 47 patients included in the analysis, 29 had preresistance (baseline) plasma samples available for analysis. We compared the time to progression (TTP) on HRD-targeted treatment (this being olaparib for all assessable cases) in patients with a resistance mechanism detected in their baseline plasma sample ($n = 5$) to those without ($n = 24$). All five patients in the former group (KCL753, 757, 477, 693 and 765) had a reversion mutation

in *BRCA1/2*. Four out of these five patients had received platinum-based chemotherapy before olaparib, which may have selected for a clone with reversion. In patients with a reversion mutation at baseline, median TTP was 2.6 months versus 7.2 months in those without (Wilcoxon rank sum $P = 0.001$; Figure 6C and Supplementary Table S18, available at <https://doi.org/10.1016/j.annonc.2024.01.003>). This raises the possibility that early ctDNA screening for HRD-targeted therapy resistance mechanisms could predict futility of such therapy and guide more appropriate treatment options for these patients. We then asked if the detection of a reversion mutation at any time point after having started treatment, but before clinical progression, was associated with a shorter TTP. In the 10 patients with intermediate samples on treatment who did not have reversions detected in their baseline samples, those with reversions ever detected ($n = 5$) had a median TTP 5.2 months versus 5.0 months when there was no detectable reversion ($n = 5$). The median time from reversion detection to resistance in this group was 3.3 months, (range 1.8-3.9 months; Wilcoxon rank sum $P = 0.8413$; Supplementary Table S18, available at <https://doi.org/10.1016/j.annonc.2024.01.003>).

Of the 40 patients for whom we collected a plasma sample directly after resistance, 33 went on to have subsequent treatment including platinum and licensed standard-of-care breast cancer chemotherapies. Time on treatment and progression status on the first subsequent treatment following HRD-targeted therapy resistance are shown with a swimmer plot for two groups—those with or without a known HRD-targeted therapy resistance mechanism detected in plasma (Figure 6D). The TTP analysis for the first subsequent treatment following HRD-targeted therapy resistance (Supplementary Figure S12, available at <https://doi.org/10.1016/j.annonc.2024.01.003>) found no significant difference (2.1 months versus 4.1 months) in TTP between groups. This analysis is underpowered to detect small effect size but raises the hypothesis that the presence of an HRD-targeted therapy resistance mechanism may predict response to HRD-targeted therapy but not to generic subsequent treatments.

DISCUSSION

The cohort investigated here represents the largest advanced breast cancer cohort for which HRD-targeted

metastasis specimen S1, S2 and S3) for analysis (a brain metastasis that was sectioned into three discrete specimens after olaparib PD). The duration of each treatment delivered in the metastatic setting is indicated in months. (D) Cross-sectional computed tomography scans (images captured in the first four panels are of the left breast) and a brain magnetic resonance imaging (fifth panel) of patient KCL709 to monitor response to treatment in the regions sampled. Times at which breast tumour specimen T1 (before olaparib), breast tumour specimen T2 (after olaparib PD) and brain metastasis specimens S1, S2 and S3 (after olaparib PD) were isolated are shown. (E) Line plot showing change in mTF and RTV across the treatment duration. (F) Line plot showing the relative presence of a *RIF1* loss-of-function mutation in KCL709 ctDNA over time. (G) Violin plot of *BRCA1* RNA levels in tumour samples obtained from KCL709. (H) Confocal microscopy images of KCL709 FFPE tumour specimens isolated before and after olaparib resistance. BRCA1 foci in geminin-positive cells are shown. Scale bar = 10 μm . (I) Quantification of (H). (J) Confocal microscopy images of KCL709 FFPE tumour specimens isolated before and after olaparib resistance. RAD51 foci in geminin-positive cells are shown. Scale bar = 10 μm . KCL004 (*BRCA1m*) is a negative control, KCL010 (*BRCAwt*) is a positive control. (K) Quantification of (J). A RAD51 score of >10% indicates homologous recombination proficiency. KCL004 (*BRCA1* mutant) is a negative control, KCL010 (*BRCAwt*) is a positive control. (L) Violin plot of *SHLD2* RNA levels in tumour samples obtained from KCL709. (M) Chromosome copy number plot illustrating partial deletion of *SHLD2* in breast tumour specimen T1 and T2 and subsequent deep deletion in brain metastasis specimens S1, S2 and S3. Copy number changes are as indicated in the key below. Blue indicates copy number loss/deletions and red indicates copy number gain/amplifications.

Ab, antibody; FFPE, formalin-fixed, paraffin-embedded; HRD, homologous recombination deficiency; mTF, methylation-based tumour fraction; PARPi, poly (ADP-ribose) polymerase (PARP) inhibitor; PD, progressive disease; PD-L1, programmed death-ligand 1; RT, radiotherapy; RNA-seq, RNA sequencing; RTV, radiologically assessed tumour volumes; wt, wild type.

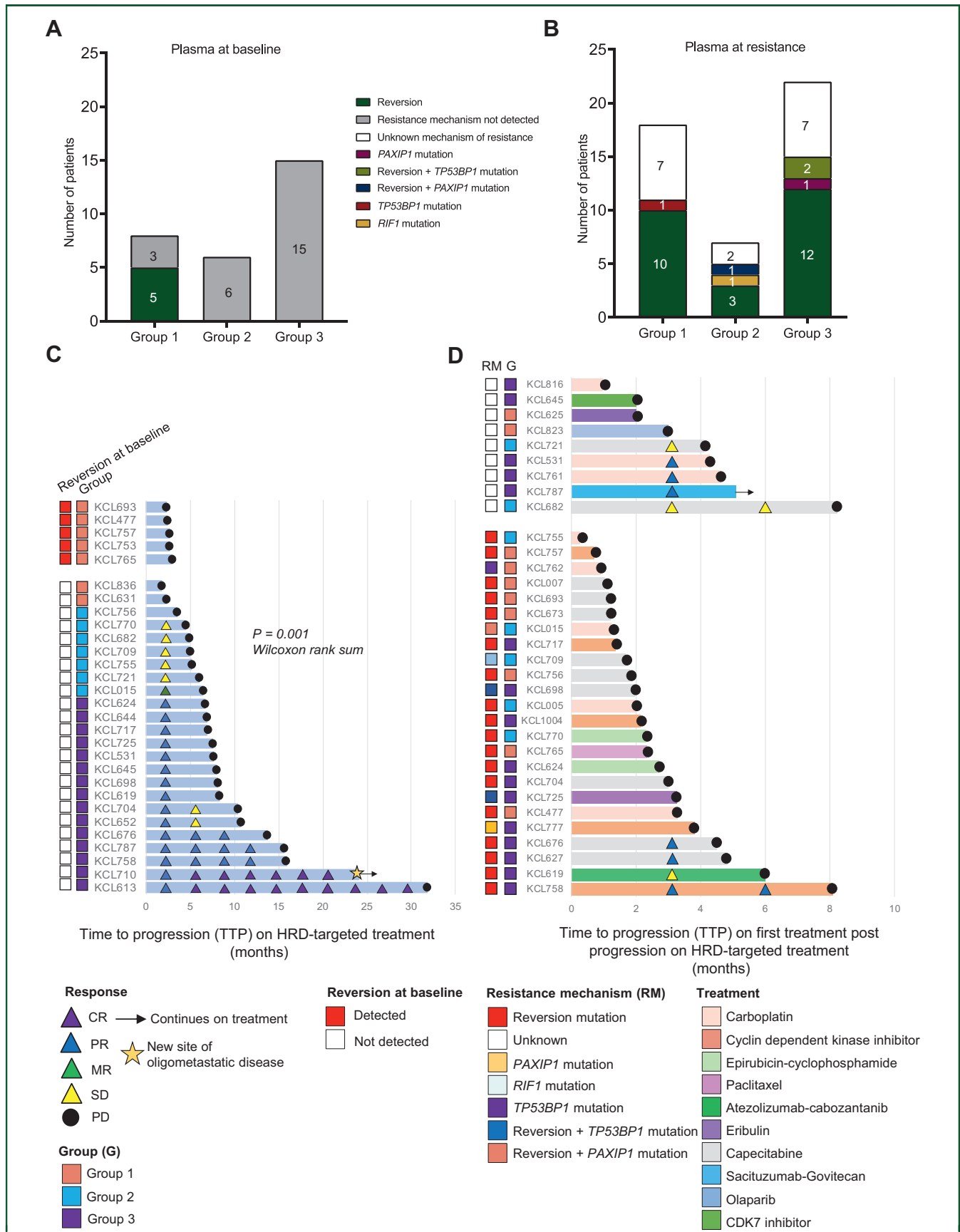


Figure 6. Reversions detected at baseline are associated with shorter time to progression on olaparib. (A) Bar chart illustrating ctDNA analysis of available pre-HRD-targeted treatment (baseline) plasma samples. Groups 1, 2 and 3 are shown; resistance mechanisms are indicated by different coloured bar segments. (B) Bar chart illustrating ctDNA analysis of plasma samples obtained from patients who have progressed on HRD-targeted treatment. Details per (A). (C) Swimmer plot showing TTP on HRD-targeted treatment. Only patients with a prerescistance plasma sample are included ($n = 29$). The data are grouped according to whether a resistance

therapy resistance, including PARPi, has been systematically investigated across time (Supplementary Figure S13, available at <https://doi.org/10.1016/j.annonc.2024.01.003>). The majority of patients received PARPi in the context of standard-of-care access arrangements, allowing us to assess the frequency of HRD-targeted resistance mechanisms in a real-world clinical breast cancer context. The frequency of reversion detections (reversions found in ctDNA in 60% of patients at progression) is higher than that in similar-sized cohorts of ovarian cancer, such as ARIEL2, where reversions were found in 19% of cfDNA samples taken after progression on rucaparib.¹³ This higher frequency could reflect the many differences between germline *BRCA*-mutant breast and ovarian cancer, in terms of both background disease biology and differing standard-of-care treatment approaches before PARPi use; in breast cancer this includes DNA-damaging adjuvant and first-line metastatic chemotherapy, often continued to progression, in contrast to the fixed duration used in advanced ovarian cancer. The methodological differences between studies for the detection and reporting of reversions could also contribute to the higher frequency of *BRCA1/2* reversion mutations detected in our study. For example, the standard clinical reporting of Guardant360CDx would have reported only 41/81 (50.6%) reversions occurring in 16/28 (57%) individuals identified with reversion mutations in our cohort (Supplementary Table S19, available at <https://doi.org/10.1016/j.annonc.2024.01.003>). It should be noted that we manually analysed GuardantINFINITY ctDNA sequencing data, beyond its standard analysis algorithms or those used in the Guardant360CDx standard reporting process, to identify reversions such as large intragenic deletions or secondary mutations that restore splice acceptor sites. This manual curation of reversions could also contribute to the higher reversion detection frequency (Figure 2D).

Inclusion of genes implicated in PARPi resistance from preclinical studies (for example *TP53BP1*, *RIF1* and *PAXIP1*) in the GuardantINFINITY panel allowed us to further assess emerging biomarkers. We observed LoF mutations in these genes in patients with acquired resistance. Such mutations were infrequent compared with reversions, and often co-occurred with reversions. We also observed copy number loss with transcript depletion of *SHLD2* across serial tumour biopsies during development of resistance (Figure 5L and M). The nature of the resistance mechanism may have implications for the use of DNA polymerase theta inhibitors and other agents that may be synthetic lethal with Shieldin pathway mutations^{53,58} or non-HR-related aspects of *BRCA1/2* deficiency. However, the clear need is to find appropriate therapeutic options for patients with reversion mutations.

Our data suggest that detection of reversions in ctDNA could be a useful clinical monitoring tool in advanced breast cancer, predicting futility of HRD-targeted therapy, given that we did not observe reversions before treatment in any of the patients that had evidence of a response to PARPi (Groups 2 and 3), but 50% of *de novo* resistant patients for whom we had a pre-PARPi plasma sample did have a reversion (Group 1; Figure 6A) and that reversion was associated with a significantly shorter TTP of 2.6 months (Figure 6C). We did not find evidence that the presence of a known HRD-targeted therapy resistance mechanism predicted TTP to more generic breast cancer chemotherapies (Figure 6D). By contrast, we did not observe a significant difference in TTP between patients with or without detectable reversion mutations detected during treatment before clinical progressive disease. However, these observations require prospective assessment to examine clinical utility of ctDNA analysis for HRD-targeted therapy response prediction.

Examination of reversions in ctDNA in large cohorts of germline carriers could inform a read-out of 'revertibility' of specific pathogenic mutations in specific contexts, providing some prediction of how and when resistance might develop. Studies in ovarian cancer have also suggested better PARPi outcomes for patients with large rearrangement or missense mutations in HR genes, events that are unlikely to be revertible.^{54,55} The cohort described here contained two patients with large deletions and one with a missense mutation, neither of whom acquired reversions. Furthermore, no patients with C-terminal *BRCA2* pathogenic mutations reverted, supporting prior observations that reversion of pathogenic mutations in this coding region are relatively rare.¹² However, we did find unconventional reversions of splice acceptor pathogenic mutations by large deletions and neofunctional splicing mutations (Figures 2 and 3). There were also mutations in regions known to support reversions (e.g. *BRCA1/2* exon 11) in our cohort that did not revert (Figure 5A). More information is therefore required to inform whether such mutations are at risk of reversion or not.

Importantly, there are still a significant number of patients where the basis of resistance remains unknown (Figure 6B). In one patient with *de novo* resistance (Group 1) to platinum, KCL625 (*PALB2m*), lack of loss of heterozygosity (LOH) at the pathogenic allele and the absence of an HRD scar (Table 1) suggest that the pretreatment tumour was not HR deficient and might explain the observed resistance to platinum-based chemotherapy. However, a separate study sequencing a later sample of cerebrospinal fluid at resistance, and an organoid derived from this sample,⁵⁹ did show evidence of *PALB2* LOH. Further study

mechanism was detected ($n = 5$) in their prerestistance (baseline) plasma sample or not ($n = 24$). Duration of HRD-targeted treatment is calculated in months; patient groups and resistance mechanisms are indicated to the left of the plot. Difference in the duration of HRD-targeted treatment between those with reversion at baseline plasma sample and those without ($P = 0.001$), Wilcoxon rank sum test. (D) Swimmer plot showing TTP on the first subsequent treatment following progression on HRD-targeted treatment. All patients with a post-HRD-targeted treatment-resistant plasma sample who went on to have subsequent treatment after plasma collection are included (33/47). Duration of treatment is calculated in months; patient groups and resistance mechanisms are indicated to the left of the plot. ctDNA, circulating tumour DNA; G, patient group; HRD, homologous recombination deficiency; RM, resistance mechanism; TTP, time to progression.

of resistance not associated with reversion mutations or absence of LOH, for example, those mediated by changes in splicing (Supplementary Figures S7 and S8, available at <https://doi.org/10.1016/j.annonc.2024.01.003> and Figures 3-5) or epigenetic mechanisms, remains an area for future research in such patients.

It is possible that additional contributions to resistance could be identified by the estimation of copy number data from ctDNA. For example, copy number loss of genes such as *TP53BP1* in *BRCA1*-mutant cancers could, conceivably, cause PARPi resistance. However, in our study we did not estimate copy number profiles from our ctDNA analysis due to the often-low fraction of ctDNA in the total cfDNA isolated from patients. Compared with the calling of mutations, robust interpretation of copy number loss from ctDNA sequencing requires >10% of the total plasma cfDNA to be ctDNA. The ctDNA fractions across our cohort's longitudinal samples were variable, with many samples not meeting this threshold. This problem could also be compounded by the possibility that some of the copy number alterations in ctDNA could be subclonal, as was the case for *BRCA1/2* reversion mutations. Based on this, we feel that reporting of copy number loss across the cohort would require a future analysis of a cohort where a higher ctDNA tumour fraction is available.

Most patients demonstrated RAD51 foci restoration at resistance, suggesting reacquisition of functional HR (Supplementary Figure S6D and E, available at <https://doi.org/10.1016/j.annonc.2024.01.003>). Our results highlight that the prevalence and multiclonality of a diverse range of reversions that drive reacquisition of HR via restoration of a functional *BRCA1/2* gene is the favoured route, but also describe for the first time other preclinically identified mechanisms identified within and across patients in resistant disease (Figures 2 and 3 and Supplementary Figures S7 and S8, available at <https://doi.org/10.1016/j.annonc.2024.01.003>). The prevention of reversion or therapies that target vulnerabilities remaining after or associated with HR restoration therefore warrants exploration. Our finding that subclonal LoF of the NHEJ pathway, which offers a new vulnerability by sensitising PARPi-resistant cells to polymerase theta inhibitors,⁵³ can coexist with *BRCA1/2* reversions suggests the need to consider multiple resistance mechanisms when considering patient selection for such approaches.

ACKNOWLEDGEMENTS

We thank the ICR Genomics Facility for sequencing support and KCL Biological Services Unit for *in vivo* studies. We thank Mark Robson, Jorge Reis-Filho and Pedram Rezavi (MSKCC), Ben O'Leary and Ros Cutts (ICR) for helpful discussions. The following figures were created with BioRender.com, with publication permission: Figures 1C, 3A, D and E; and Supplementary Figures S9A, S9B, S9C, S11A and S13.

FUNDING

This work was funded by Breast Cancer Now through the Breast Cancer Now Toby Robins Research Centre (CTR-Q5-Y3)

to ANJT and CJL, a Programme Grant from Cancer Research UK to CJL and ANJT (DRCRPGNov21y100001) and through Breast Cancer Research Foundation (BCRF-23-199) to ANJT. EHJ was supported by a fellowship funded by Cancer Research UK and AstraZeneca. Guardant Health provided plasma ctDNA sequencing.

DISCLOSURE

ANJT is/has been a consultant for AstraZeneca, Merck KGaA, Artios, Pfizer, Vertex, GE Healthcare, Inbiomotion, Prime Oncology, Medscape Education, EMPartners, VJ Oncology, Gilead and MD Anderson Cancer Centre; has received grant/research support from AstraZeneca, Myriad, Medivation and Merck KGaA; is a stockholder in Inbiomotion; is also a named inventor on patents describing the use of DNA repair inhibitors and stands to gain from their development and use as part of the ICR 'Rewards to Inventors' scheme and also reports benefits from this scheme associated with patents for PARP inhibitors paid to ANJT ANJT research accounts at the Institute of Cancer Research. CJL receives and/or has received research funding from AstraZeneca, Merck KGaA and Artios; received consultancy, SAB membership or honoraria payments from Syncona, Sun Pharma, Gerson Lehrman Group, Merck KGaA, Vertex, AstraZeneca, Tango, 3rd Rock, Ono Pharma, Artios, Abingworth, Tesselate, Dark Blue Therapeutics, Pontifax, Astex, Neophore, Glaxo Smith Kline; has stock in Tango, Ovibio, Hysplex and Tesselate; is also a named inventor on patents describing the use of DNA repair inhibitors and stands to gain from their development and use as part of the ICR 'Rewards to Inventors' scheme and also reports benefits from this scheme associated with patents for PARP inhibitors paid into CJL's personal account and research accounts at the Institute of Cancer Research. AY, JY, MD, and LD are employees and stockholders of Guardant Health. JY is a former full-time employee at Guardant Health and a current full-time employee at Exai Bio. SJP is a named inventor on patents relating to targeting PARPi resistance and stands to gain from their development and use as part of the ICR 'Rewards to Inventors' scheme. VS has research grants and receives honoraria from AstraZeneca. ALG and VS are co-inventors of the patent PCT/EP2018/086759 (WO2019122411A1). VS and ALG received funding from Fundació La Marató de TV3 (654/C/2019), FERO-GHD and AECC (INVES20095LLOP). NL is employed by AstraZeneca and owns AstraZeneca stock. The other authors declare no conflict of interest.

REFERENCES

- Farmer H, McCabe N, Lord CJ, et al. Targeting the DNA repair defect in BRCA mutant cells as a therapeutic strategy. *Nature*. 2005;434(7035):917-921.
- Bryant HE, Schultz N, Thomas HD, et al. Specific killing of BRCA2-deficient tumours with inhibitors of poly(ADP-ribose) polymerase. *Nature*. 2005;434(7035):913-917.
- Robson M, Im S-A, Senkus E, et al. Olaparib for metastatic breast cancer in patients with a germline BRCA mutation. *N Engl J Med*. 2017;377(6):523-533.

4. Litton JK, Rugo HS, Ettl J, et al. Talazoparib in patients with advanced breast cancer and a germline BRCA mutation. *N Engl J Med*. 2018;379(8):753-763.
5. Staaf J, Glodzik D, Bosch A, et al. Whole-genome sequencing of triple-negative breast cancers in a population-based clinical study. *Nat Med*. 2019;25(10):1-23.
6. Geyer CE, Sikov WM, Huober J, et al. Long-term efficacy and safety of addition of carboplatin with or without veliparib to standard neoadjuvant chemotherapy in triple-negative breast cancer: 4-year follow-up data from BrighTNess, a randomized phase III trial. *Ann Oncol*. 2022;33(4):384-394.
7. Tutt ANJ, Garber JE, Kaufman B, et al. Adjuvant olaparib for patients with BRCA1- or BRCA2-mutated breast cancer. *N Engl J Med*. 2021;384(25):2394-2405.
8. Geyer CE Jr, Garber JE, Gelber RD, et al. Overall survival in the OlympiA phase III trial of adjuvant olaparib in patients with germline pathogenic variants in BRCA1/2 and high-risk, early breast cancer. *Ann Oncol*. 2022;33(12):1250-1268.
9. Lord CJ, Ashworth A. PARP inhibitors: synthetic lethality in the clinic. *Science*. 2017;355(6330):1152-1158.
10. Edwards SL, Brough R, Lord CJ, et al. Resistance to therapy caused by intragenic deletion in BRCA2. *Nature*. 2008;451(7182):1111-1115.
11. Sakai W, Swisher EM, Karlan BY, et al. Secondary mutations as a mechanism of cisplatin resistance in BRCA2-mutated cancers. *Nature*. 2008;451(7182):1116-1120.
12. Pettitt SJ, Frankum JR, Punta M, et al. Clinical BRCA1/2 reversion analysis identifies hotspot mutations and predicted neoantigens associated with therapy resistance. *Cancer Discov*. 2020;10(10):1475-1488.
13. Lin KK, Harrell MI, Oza AM, et al. BRCA reversion mutations in circulating tumor DNA predict primary and acquired resistance to the PARP inhibitor rucaparib in high-grade ovarian carcinoma. *Cancer Discov*. 2019;9(2):210-219.
14. Quigley D, Alumkal JJ, Wyatt AW, et al. Analysis of circulating cell-free DNA identifies multiclonal heterogeneity of BRCA2 reversion mutations associated with resistance to PARP inhibitors. *Cancer Discov*. 2017;7(9):999-1005.
15. Goodall J, Mateo J, Yuan W, et al. Circulating cell-free DNA to guide prostate cancer treatment with PARP inhibition. *Cancer Discov*. 2017;7(9):1006-1017.
16. Kondrashova O, Nguyen M, Shield-Artin K, et al. Secondary somatic mutations restoring RAD51C and RAD51D associated with acquired resistance to the PARP inhibitor rucaparib in high-grade ovarian carcinoma. *Cancer Discov*. 2017;7(9):984-998.
17. Tobalina L, Armenia J, Irving E, O'Connor MJ, Forment JV. A meta-analysis of reversion mutations in BRCA genes identifies signatures of DNA end-joining repair mechanisms driving therapy resistance. *Ann Oncol*. 2021;32(1):103-112.
18. Wicks AJ, Krastev DB, Pettitt SJ, Tutt ANJ, Lord CJ. Opinion: PARP inhibitors in cancer-what do we still need to know? *Open Biol*. 2022;12(7):220118.
19. Dev H, Chiang T-WW, Lescale C, et al. Shieldin complex promotes DNA end-joining and counters homologous recombination in BRCA1-null cells. *Nat Cell Biol*. 2018;20(8):954-965.
20. Noordermeer SM, Adam S, Setiaputra D, et al. The shieldin complex mediates 53BP1-dependent DNA repair. *Nature*. 2018;560(7716):117-121.
21. Gupta R, Somyajit K, Narita T, et al. DNA repair network analysis reveals shieldin as a key regulator of NHEJ and PARP inhibitor sensitivity. *Cell*. 2018;173(4):972-988.e23.
22. Mirman Z, Lottersberger F, Takai H, et al. 53BP1-RIF1-shieldin counteracts DSB resection through CST- and Pol α -dependent fill-in. *Nature*. 2018;560(7716):112-116.
23. Drané P, Brault M-E, Cui G, et al. TIRR regulates 53BP1 by masking its histone methyl-lysine binding function. *Nature*. 2017;543(7644):211-216.
24. Xu G, Chapman JR, Brandsma I, et al. REV7 counteracts DNA double-strand break resection and affects PARP inhibition. *Nature*. 2015;521(7553):541-544.
25. Ray Chaudhuri A, Callen E, Ding X, et al. Replication fork stability confers chemoresistance in BRCA-deficient cells. *Nature*. 2016;535(7612):382-387.
26. Murai J, Huang S-YN, Das BB, et al. Trapping of PARP1 and PARP2 by clinical PARP inhibitors. *Cancer Res*. 2012;72(21):5588-5599.
27. Krastev DB, Li S, Sun Y, et al. The ubiquitin-dependent ATPase p97 removes cytotoxic trapped PARP1 from chromatin. *Nat Cell Biol*. 2022;24(1):62-73.
28. Pettitt SJ, Krastev DB, Brandsma I, et al. Genome-wide and high-density CRISPR-Cas9 screens identify point mutations in PARP1 causing PARP inhibitor resistance. *Nat Commun*. 2018;9(1):1849.
29. Patch A-M, Christie EL, Etemadmoghadam D, et al. Whole-genome characterization of chemoresistant ovarian cancer. *Nature*. 2015;521(7553):489-494.
30. Christie EL, Pattnaik S, Beach J, et al. Multiple ABCB1 transcriptional fusions in drug resistant high-grade serous ovarian and breast cancer. *Nat Commun*. 2019;10(1):1295.
31. Rottenberg S, Jaspers JE, Kersbergen A, et al. High sensitivity of BRCA1-deficient mammary tumors to the PARP inhibitor AZD2281 alone and in combination with platinum drugs. *Proc Natl Acad Sci U S A*. 2008;105(44):17079-17084.
32. Cruz C, Castroviejo-Bermejo M, Gutiérrez-Enríquez S, et al. RAD51 foci as a functional biomarker of homologous recombination repair and PARP inhibitor resistance in germline BRCA-mutated breast cancer. *Ann Oncol*. 2018;29(5):1203-1210.
33. Davies H, Glodzik D, Morganella S, et al. HRDetect is a predictor of BRCA1 and BRCA2 deficiency based on mutational signatures. *Nat Med*. 2017;23(4):517-525.
34. Lefebvre C, Bachelot T, Filleron T, et al. Mutational profile of metastatic breast cancers: a retrospective analysis. *PLoS Med*. 2016;13(12):e1002201.
35. Wood RD, Mitchell M, Sgouros J, Lindahl T. Human DNA repair genes. *Science*. 2001;291(5507):1284-1289.
36. Wood RD, Mitchell M, Lindahl T. Human DNA repair genes, 2005. *Mutat Res*. 2005;577(1-2):275-283.
37. Lange SS, Takata K-I, Wood RD. DNA polymerases and cancer. *Nat Rev Cancer*. 2011;11(2):96-110.
38. He YJ, Meghani K, Caron M-C, et al. DYNLL1 binds to MRE11 to limit DNA end resection in BRCA1-deficient cells. *Nature*. 2018;563(7732):522-526.
39. Jaspers JE, Kersbergen A, Boon U, et al. Loss of 53BP1 causes PARP inhibitor resistance in Brca1-mutated mouse mammary tumors. *Cancer Discov*. 2013;3(1):68-81.
40. Chapman JR, Barral P, Vannier J-B, et al. RIF1 Is Essential for 53BP1-dependent nonhomologous end joining and suppression of DNA double-strand break resection. *Mol Cell*. 2021;81(13):2868.
41. Barazas M, Annunziato S, Pettitt SJ, et al. The CST complex mediates end protection at double-strand breaks and promotes PARP inhibitor sensitivity in BRCA1-deficient cells. *Cell Rep*. 2018;23(7):2107-2118.
42. Gogola E, Duarte AA, de Ruiter JR, et al. Selective loss of PARG restores PARylation and counteracts PARP inhibitor-mediated synthetic lethality. *Cancer Cell*. 2019;35(6):950-952.
43. Datta A, Biswas K, Sommers JA, et al. WRN helicase safeguards deprotected replication forks in BRCA2-mutated cancer cells. *Nat Commun*. 2021;12(1):6561.
44. Mirza MR, Monk BJ, Herrstedt J, et al. Niraparib maintenance therapy in platinum-sensitive, recurrent ovarian cancer. *N Engl J Med*. 2016;375(22):2154-2164.
45. Coleman RL, Oza AM, Lorusso D, et al. Rucaparib maintenance treatment for recurrent ovarian carcinoma after response to platinum therapy (ARIEL3): a randomised, double-blind, placebo-controlled, phase 3 trial. *Lancet*. 2017;390(10106):1949-1961.
46. Patel JN, Braicu I, Timms KM, et al. Characterisation of homologous recombination deficiency in paired primary and recurrent high-grade serous ovarian cancer. *Br J Cancer*. 2018;119(9):1060-1066.
47. Nesić K, Kondrashova O, Hurley RM, et al. Acquired RAD51C promoter methylation loss causes PARP inhibitor resistance in high-grade serous ovarian carcinoma. *Cancer Res*. 2021;81(18):4709-4722.
48. Murciano-Goroff YR, Schram AM, Rosen EY, et al. Reversion mutations in germline BRCA1/2-mutant tumors reveal a BRCA-mediated phenotype in non-canonical histologies. *Nat Commun*. 2022;13(1):7182.
49. Tutt A, Tovey H, Cheang MCU, et al. Carboplatin in BRCA1/2-mutated and triple-negative breast cancer BRCAness subgroups: the TNT Trial. *Nat Med*. 2018;24(5):628-637.

50. Bunting SF, Call n E, Wong N, et al. 53BP1 inhibits homologous recombination in Brca1-deficient cells by blocking resection of DNA breaks. *Cell*. 2010;141(2):243-254.
51. Bouwman P, Aly A, Escandell JM, et al. 53BP1 loss rescues BRCA1 deficiency and is associated with triple-negative and BRCA-mutated breast cancers. *Nat Struct Mol Biol*. 2010;17(6):688-695.
52. Cao L, Xu X, Bunting SF, et al. A selective requirement for 53BP1 in the biological response to genomic instability induced by Brca1 deficiency. *Mol Cell*. 2009;35(4):534-541.
53. Zatreanu D, Robinson HMR, Alkhatib O, et al. Pol  inhibitors elicit BRCA-gene synthetic lethality and target PARP inhibitor resistance. *Nat Commun*. 2021;12(1):3636.
54. Swisher EM, Kristeleit RS, Oza AM, et al. Characterization of patients with long-term responses to rucaparib treatment in recurrent ovarian cancer. *Gynecol Oncol*. 2021;163(3):490-497.
55. Sullivan MR, Prakash R, Rawal Y, et al. Long-term survival of an ovarian cancer patient harboring a RAD51C missense mutation. *Cold Spring Harb Mol Case Stud*. 2021;7(2):a006083.
56. Tung N, Miron A, Schnitt SJ, et al. Prevalence and predictors of loss of wild type BRCA1 in estrogen receptor positive and negative BRCA1-associated breast cancers. *Breast Cancer Res*. 2010;12(6):R95.
57. Dworkin AM, Spearman AD, Tseng SY, Sweet K, Toland AE. Methylation not a frequent "second hit" in tumors with germline BRCA mutations. *Fam Cancer*. 2009;8(4):339-346.
58. Zhou J, Gelot C, Pantelidou C, et al. A first-in-class polymerase theta inhibitor selectively targets homologous-recombination-deficient tumors. *Nat Cancer*. 2021;2(6):598-610.
59. Fitzpatrick A, Iravani M, Mills A, et al. Genomic profiling and pre-clinical modelling of breast cancer leptomeningeal metastasis reveals acquisition of a lobular-like phenotype. *Nat Commun*. 2023;14(1):1-18.